Astroparticle Physics

Lectures:

05.02.2019 1. Historical introduction, basic properties of cosmic rays
07.02.2019 2. Hadronic interactions and accelerator data
19.02.2019 3. Cascade equations
21.02.2019 4. Electromagnetic cascades
26.02.2019 5. Extensive air showers
28.02.2019 6. Detectors for extensive air showers
09.04.2019 7. High energy cosmic rays and the knee in the energy spectrum of cosmic rays
16.04.2019 8. Radio detection of extensive air showers
25.04.2019 9. Acceleration, astrophysical accelerators and beam dumps
07.05.2019 10. Extragalactic propagation of cosmic rays
16.05.2019 11. Ultra high energy cosmic rays
21.05.2019 12. Astrophysical gamma rays and neutrinos
28.05.2019 13. Neutrino astronomy
04.06.2019 14. Gamma-ray astronomy

http://particle.astro.ru.nl/goto.html?astropart1819

lecture 13
Neutrino astronomy
Gaisser chapter 18

Because neutrinos interact only by the weak interaction, a large target volume is necessary to detect them. This is especially true in the case of naturally occurring neutrinos where the flux is low compared to neutrinos from an accelerator beam or from a nuclear reactor. The idea of using a large volume of clear water to detect neutrinos was proposed in 1960 by Greisen [538], Reines [693] and Markov [694]. The Cherenkov light from charged particles produced by interactions of neutrinos would be detected by optical modules in the water, visible from a long distance. Reines distinguished between cosmic neutrinos (by which he meant neutrinos of astrophysical origin) and cosmic ray (i.e. atmospheric) neutrinos. He writes that interest in the possibility of detecting cosmic neutrinos "stems from the weak interaction of neutrinos with matter, which means that they propagate essentially unchanged in direction and energy from their point of origin (except for the gravitational interaction with bulk matter, as in the case of light passing by a star) and so carry information which may be unique in character." In the same volume of Annual Reviews, Greisen proposed to use a large volume of water in a mine to detect astrophysical neutrinos. Markov proposed using the deep ocean or water in a lake to study atmospheric neutrinos.

The idea developed in two ways. The first, originally motivated by the goal of detecting proton decay, led to the relatively densely instrumented detectors in deep mines, IMB and Kamiokande, which detected the burst of $\approx$10 MeV neutrinos from SN1987A [401, 403] and set limits on stability of the proton. The second-generation water detectors Super-Kamiokande and SNO (Sudbury Neutrino Observatory) were designed in large part for high-resolution measurements respectively of atmospheric and of solar neutrinos. Super-K confirmed oscillations of atmospheric neutrinos [59] as the cause of the anomalous ratio of ν_μ/ν_e found earlier by Kamiokande and IMB. It also set stronger limits on proton decay. SNO, filled with heavy water, measured neutral current interactions of all flavors of neutrinos from the Sun, as well as charged current interactions of ν_e, thereby confirming oscillations as the explanation of the solar neutrino problem [233, 695].

The other path was motivated by the goal of using high-energy neutrinos as a probe of cosmic ray origin. The first serious effort to build a gigaton-scale water detector to search for astrophysical neutrinos was the Deep Underwater Muon and Neutrino Detector (DUMAND) project, proposed in the 1970s. The basic ideas for designing a neutrino telescope stem from studies for DUMAND, which are documented in a series of proceedings volumes, for example [696]. Although DUMAND itself was realized only by deployment of a single string in the ocean from a ship for a few days in 1987 [697], the DUMAND effort provided the basic strategies for neutrino astronomy.

18.1 Motivation for a kilometer-scale neutrino telescope

To see what motivates the gigaton-scale, one approach is to compare with sources of TeV γ-rays. If the photons come from decay of neutral pions, as may be the case for some supernova remnants and some blazars, then we would expect a similar flux of neutrinos from decay of charged pions. Bright sources typically have fluxes less than the Crab Nebula, which is

$$\mathrm{d}N_\nu/\mathrm{d}\ln(E) \approx 3 \times 10^{-11}\mathrm{cm}^{-2}\mathrm{s}^{-1}$$

at a TeV. The blazar Mrk421 with variable flux that is sometimes almost at the Crab level is a good example [698] (see also Section 14.2.3). At this energy the neutrino cross section is $\sim 10^{-35}$ cm^2. One km^3 of water contains 6×10^{38} target nucleons, so we estimate a rate of ~ 10 neutrino interactions per year from such a source per decade of energy. From Figure 8.7 we estimate a comparable background of atmospheric neutrinos within 1°, the typical angular resolution expected for a neutrino-induced muon. A more detailed comparison between signal and background for the diffuse flux of neutrinos produced by cosmic ray interactions in the disk of the Milky Way was given in Section 11.4.

A more general argument is to relate the expected neutrino flux to the observed flux of cosmic rays [699]. The Waxman–Bahcall upper bound [700] is the benchmark example of this approach.[1] The basic idea is to start with an estimate of the cosmic ray spectrum in the sources obtained from the measured flux, as in the extragalactic case discussed in Section 17.4.1. If the sources are optically thin for the $p + \gamma \rightarrow \pi + N + X$ reactions in which neutrinos (from decay of $\pi^{\pm}$) and photons (from decay of π^0) are produced, then the energy flux of neutrinos cannot be greater than that of the cosmic rays. The original limit has to be adjusted for the effect of neutrino oscillations, and there are uncertainties related to the cosmological evolution of the sources and to the mechanism for neutrino production. The basic result is, however, that the upper limit is close to the observed energy

flux of cosmic rays in Eq. 17.1. Folding a similar astrophysical neutrino flux with $P(E_\nu, E_\mu > 100\,\mathrm{GeV})$ from Figure 8.5 leads to an estimate of $\sim$ 100 neutrino-induced muons per km^2 per year from below the horizon with $E_\mu > 100$ GeV at the detector. The expected number of astrophysical neutrinos interacting inside a gigaton volume per year is slightly smaller. Details will be discussed in connection with Figure 18.2 below.

18.2 From DUMAND to IceCube and beyond

The first successful neutrino telescopes were Baikal and then AMANDA.[2] Though much smaller than the gigaton scale, they proved the concept by detecting and measuring atmospheric neutrinos. The Lake Baikal neutrino telescope "NT200" with a volume of about a Megaton was constructed between 1993 and 1999 and has been in operation since then [704]. The original idea of DUMAND to construct a neutrino telescope in the deep ocean was first realized with the ANTARES detector [705], which began full operation with 12 lines of optical modules in the Mediterranean Sea near Toulon in 2008. The motion of the optical modules in the sea currents is monitored with a system of sonar detectors. It has a volume of more than 10 megatons.

The idea of using ice as the target was suggested by Halzen and others in 1988 [706, 707]. The history of the construction and operation of the Antarctic Muon and Neutrino Detector Array (AMANDA) is given in Ref. [708]. The technique for deploying optical modules in ice is to drill with hot water under high pressure. Four strings called "AMANDA-A" were deployed in the 1993–1994 season at the South Pole. The ice at that depth turned out to have too many air bubbles to allow reconstruction of the events because the light was scattered too much. In the deeper ice the higher pressure forces the air into the structure of the ice, and the remaining scattering is primarily due to dust. AMANDA-II was deployed over four seasons starting in 1995–96. When it was complete in 2000, AMANDA-II consisted of 19 strings with a total of 677 optical modules viewing more than 15 megatons. Analog signals were sent to the surface over a mixture of copper and optical fiber cables to electronics modules in the Martin A. Pomerantz Observatory. Data were recorded on tape and sent at the beginning of each Austral summer season for reconstruction and analysis of events in the North. Searches for neutrino sources with AMANDA alone cover the period from 2000 to 2006 [709]. The results of AMANDA are nicely summarized in Ref. [450] in the broad context of galactic and extragalactic neutrino astronomy. AMANDA continued to run as a sub-array of IceCube until it was shut off on May 11, 2009. String 18 of AMANDA was equipped and used to test the digital technology for IceCube [710].

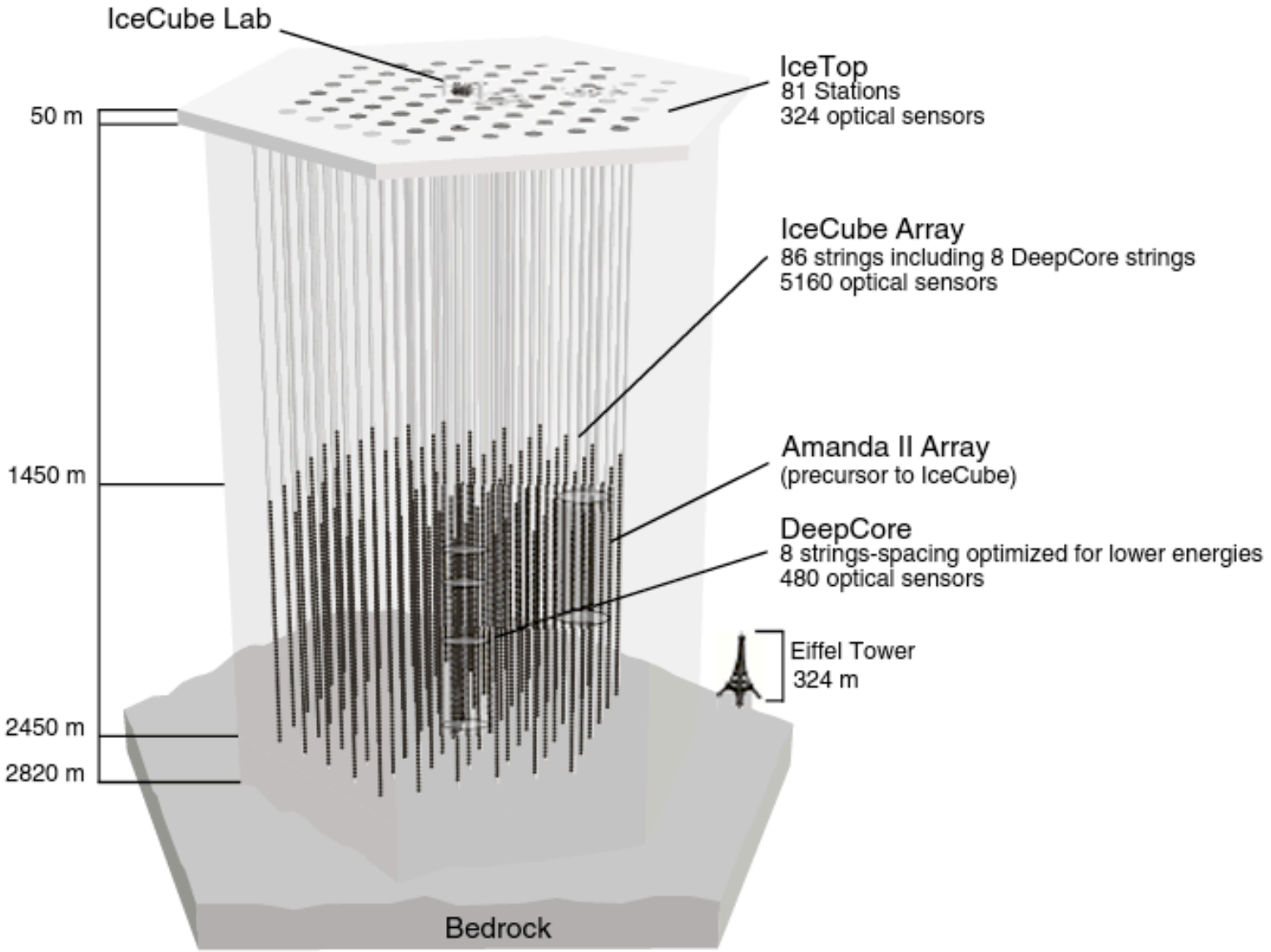

Figure 18.1 Layout of the IceCube Observatory at the South Pole. (Figure courtesy of the IceCube Collaboration.)

IceCube is the first kilometer-scale detector. An overview of its construction and early results, including the first observation of high-energy astrophysical neutrinos is given in Ref. [711]. IceCube consists of 86 vertical cables (strings) each instrumented with 60 digital optical modules (DOMs) at 17 m intervals between 1450 and 2450 meters below the surface. Signals are digitized and time-stamped in the DOMs and sent to the surface for processing [712]. Preliminary event reconstruction is done online by computers in the IceCube Lab (ICL) at the South Pole. Selected data (about 10% of physics events) are transmitted to the North by satellite for further processing. On the surface near the top of each string is a pair of tanks, separated from each other by 10 meters with two DOMs in each tank to form a km^2 air shower array, IceTop [654]. IceTop signals are fully integrated into the IceCube data acquisition system to form a three-dimensional array as shown in Figure 18.1.

Recently discovered evidence for high-energy astrophysical neutrinos by IceCube [327, 713] is motivating development of neutrino detectors of still larger effective volume. Construction of KM3NeT in the Mediterranean Sea is starting [714, 715], and plans for a second generation IceCube are being discussed [716].

18.3 Signals and backgrounds in a neutrino detector

Most of the ingredients needed to understand the strategies for neutrino astronomy are described in Chapter 8 on muons and neutrinos underground. The classic approach is to look for upward muons from charged current interactions of muon neutrinos. From Figure 8.1, we see that the rate of muons from above is about six orders of magnitude higher than the level of muons from interactions of atmospheric ν_μ at 1500 m, which corresponds to the top layers of IceCube. The figure also demonstrates that a deeper detector will have a lower background of atmospheric muons. In addition, the crossover of the atmospheric muons with the neutrino-induced muons is farther above the horizon at greater depth. From Figures 8.4 and 8.6 we also see that the Earth becomes increasingly opaque to neutrinos as energy increases above 10 TeV.

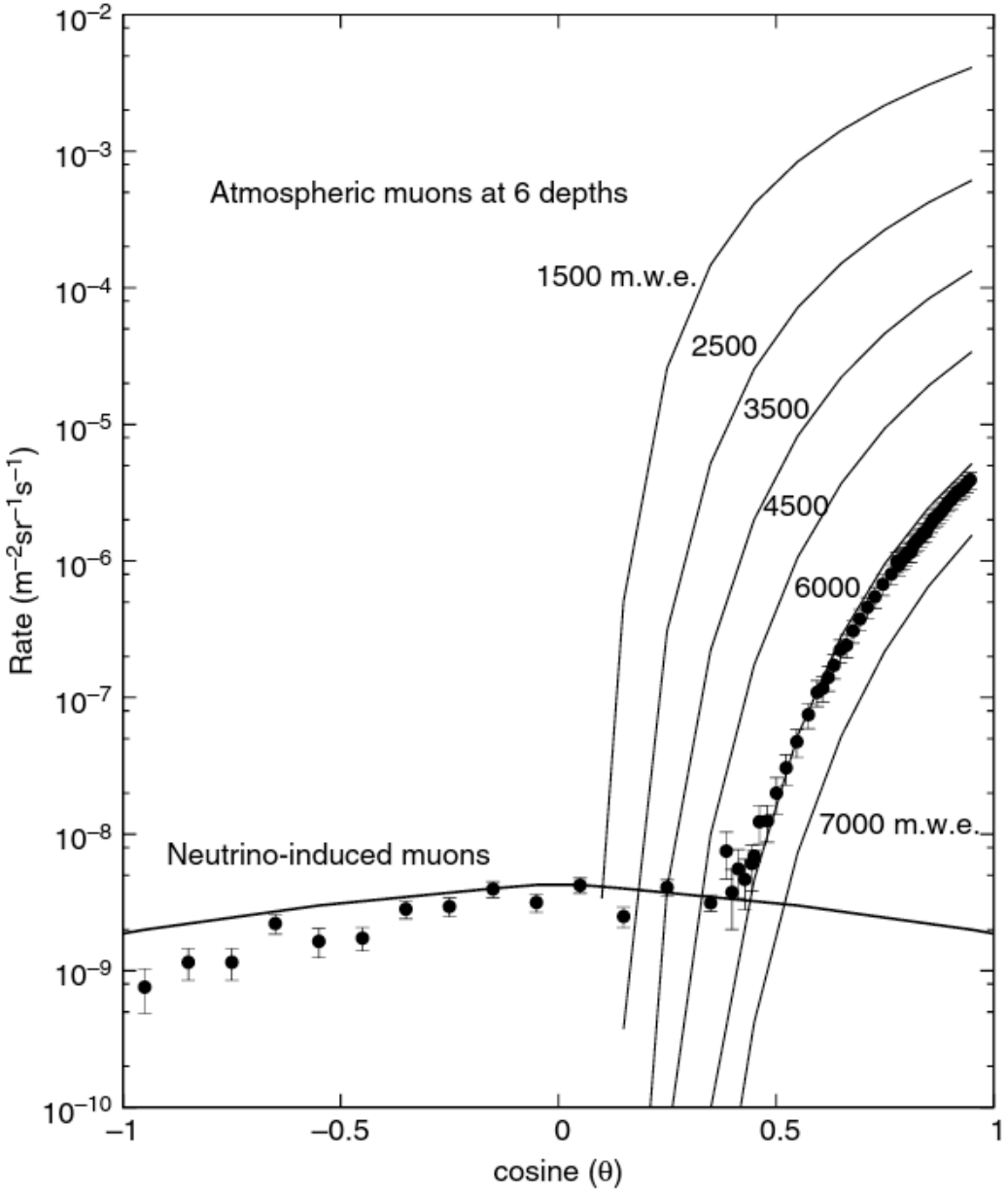

Figure 8.1 Angular dependence of the muon flux deep underground, including ν_μ-induced muons. Data are from the SNO detector at 5.89 km.w.e. [255].

With the very high proportion of atmospheric muons at moderate depths in a large detector like IceCube, the main background after the first pass selection of upward events is caused by nearly coincident downward muons. Depending on their relative timing and location, they can be reconstructed as upward moving in early levels of reconstruction. More advanced selection techniques are required to remove this background. To get an idea of the level of the problem, consider that the rate of reconstructable muons in IceCube is more than 2 kHz, with seasonal variations of $\approx \pm 10\%$. A relevant time window is the time for a particle to go diagonally across the detector, 5 μs. At 2 kHz every muon has a 1% chance of having an accidental companion. If half of these have the first muon cross below the second, then the estimated rate of events misreconstructed as upward is about 10 Hz, compared to a true rate of neutrino-induced upward muons of about 5 milli-Hz (from Figure 18.2).

In Figure 8.3, the energy spectrum of atmospheric muons deep underground is compared with that of atmospheric neutrino-induced muons. In the atmospheric case, the muons from neutrinos have a softer spectrum. This is a consequence of the very steep spectrum of atmospheric neutrinos, and would not be the case for an astrophysical component with a harder spectrum.

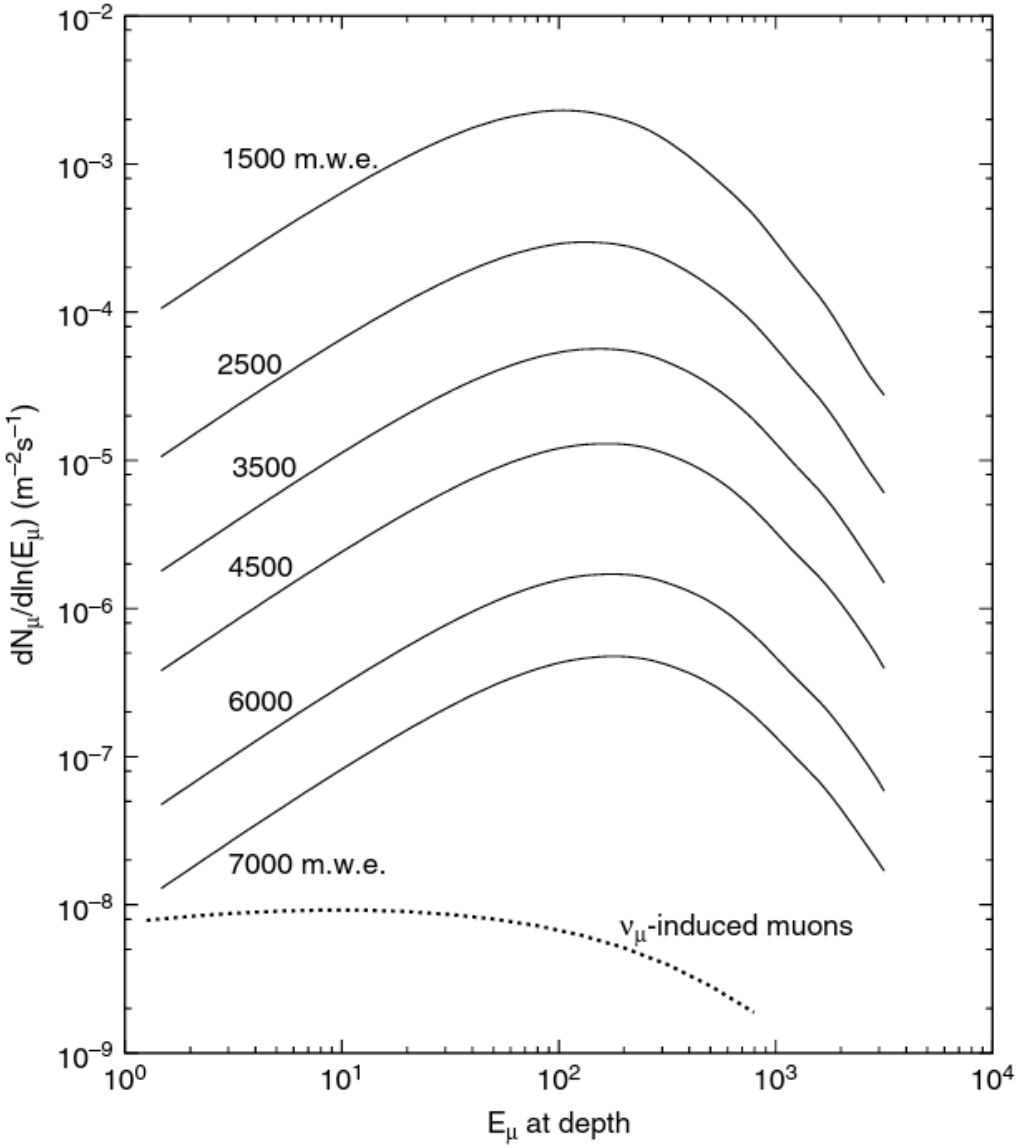

Figure 8.3 Differential energy spectrum of muons at various depths underground. The dotted line is the spectrum of neutrino-induced muons. Total rates integrated over all directions are given.

To illustrate the effect of the shape of the neutrino spectrum, we compare rates of atmospheric and astrophysical neutrinos with each other in Figure 18.2. For entering muons from ν_μ interactions we plot the rate per km^2 per sr, which is obtained by calculating

$$\phi_\nu \times P_\nu(E_\nu, E_\mu > 100\,\mathrm{GeV}),$$

where P_ν is from Figure 8.5 and $\phi_\nu = \mathrm{d}N_{\nu_\mu} / \mathrm{d}\ln(E_\nu)$. For electron neutrinos we calculate the rate per gigaton by multiplying ϕ_{ν_e} by the number of target nucleons per gigaton and by the cross section per nucleon (charged current only here) from Ref. [97]. For astrophysical neutrinos, we take a generic E^{-2} spectrum normalized by the IceCube discovery as $E_\nu\phi_\nu = 100\,\mathrm{km}^{-2}\mathrm{s}^{-1}\mathrm{sr}^{-1}$ per flavor [327]. For atmospheric neutrinos we plot the fluxes at the typical zenith angle of $\cos\theta = 0.25$ from Ref. [213] extrapolated above 10 TeV with a differential spectral index of -3.7.

Thus a potential signature of astrophysical neutrinos is a hard component of the neutrino spectrum emerging above the steeply falling atmospheric background.

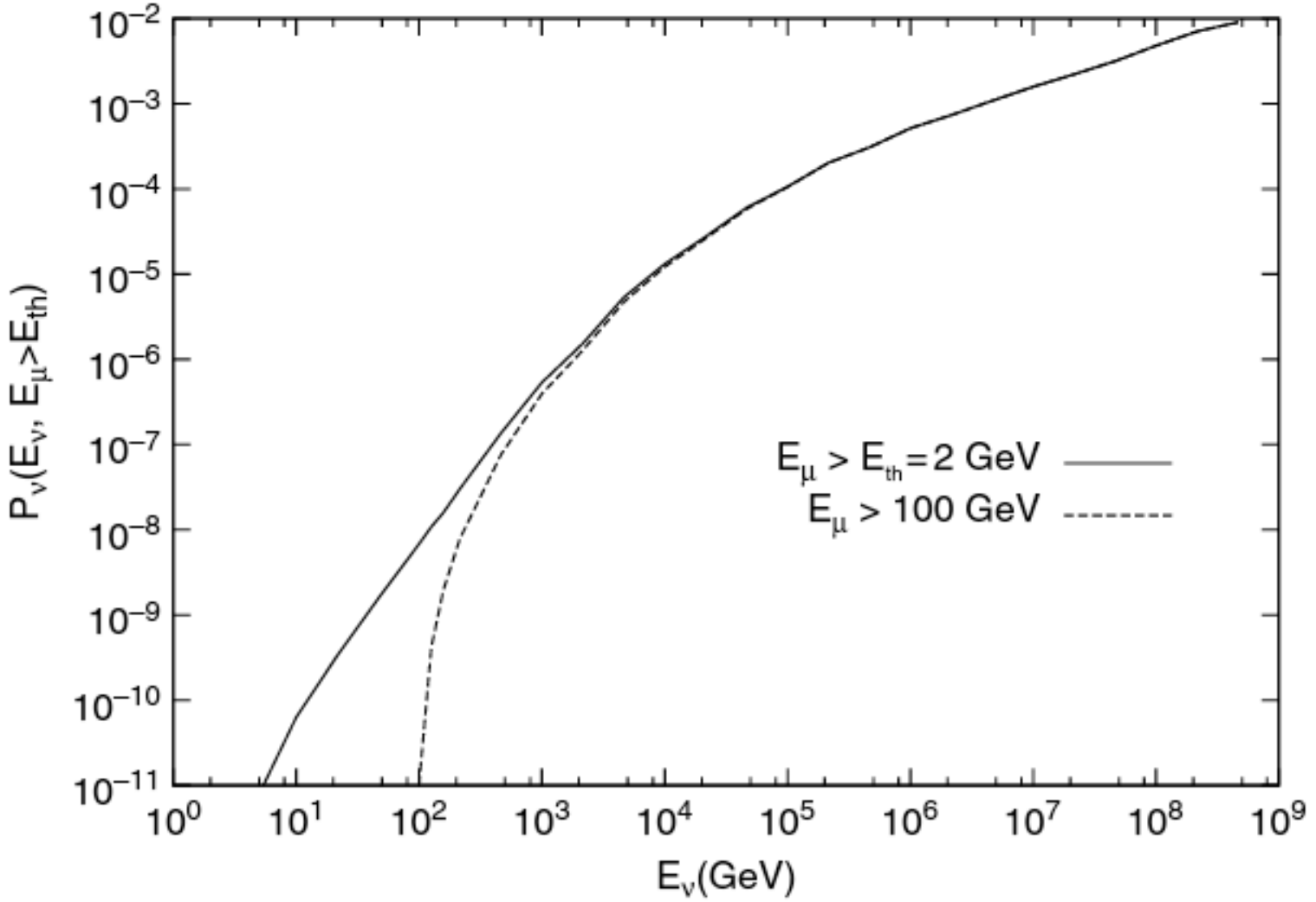

Figure 8.5 $P(E_\nu, E_\mu > E_{\rm th})$ for $E_{\rm th} = 2$ GeV (solid) and $E_{\rm th} = 100$ GeV (dashed).

Discussion: Astrophysical neutrinos are expected to have a harder spectrum at high energy than atmospheric neutrinos because they reflect the parent spectrum at the distant source. The atmospheric neutrino spectrum is steeper for two reasons. First, production of parent mesons reflects the spectrum of the local cosmic ray spectrum after propagation in the Galaxy. In addition, the spectrum of atmospheric neutrinos is further suppressed at high energy because of re-interaction of the parent mesons.

It is important to note that the rates in Figure 18.2 are plotted vs neutrino energy. In general, the energy observed in the detector is a lower limit to the energy of the neutrino. In the case of electron neutrinos, the full energy of the neutrino is deposited near the interaction vertex in the case of charged current interactions. For neutral current interactions, the energy carried away by the neutrino is lost. In the case of entering muons only the energy deposited in the detector as the muon passes through can be measured. In this case, there are two random steps: the fraction of neutrino energy carried by the muon and the fraction of the muon energy deposited in the detector. It is therefore necessary to unfold the neutrino spectrum from the distribution of observed energies based on known properties of the differential neutrino cross sections and of energy loss by muons. A straightforward approach is to assume an atmospheric neutrino spectrum and an astrophysical

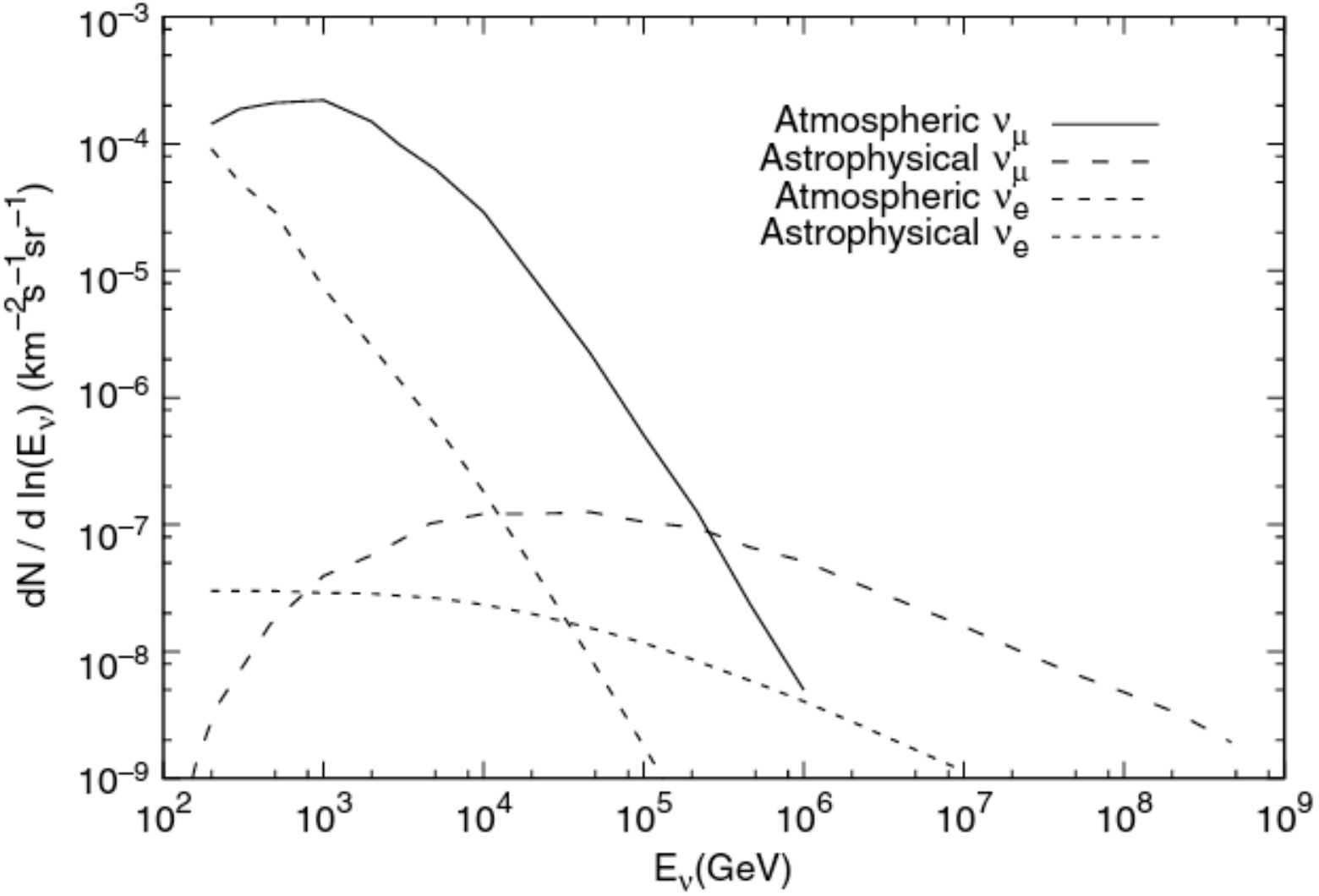

Figure 18.2 Rates of neutrino events in a kilometer-scale detector. See text for explanation and discussion.

neutrino spectrum, calculate the expected spectrum of deposited energy and compare with the distribution observed in the detector. The astrophysical spectrum is characterized by a normalization and a spectral shape to be fitted. The atmospheric background may also be characterized by nuisance parameters, usually constrained to vary within a limited range to reflect uncertainties in the primary spectrum and composition and in the parameters of neutrino production, such as the K/π ratio.

An important uncertainty that remains unresolved at the time of writing is the level of prompt atmospheric neutrinos from decay of charm. As illustrated in Figure 8.9, this component has a harder spectrum than conventional atmospheric neutrinos from decay of charged kaons and pions. Moreover, depending on the normalization of the charm component, the prompt flux is likely to become important in the same energy region where the astrophysical flux crosses the atmospheric flux.

18.4 Event types

There are two basic event types in a large neutrino detector: tracks and cascades, illustrated in Figure 18.3 by one event of each type found by IceCube [327]. Tracks are produced by muons from charged-current interactions of ν_μ. Tracks may enter the detector from interactions in the surrounding material or they can start inside the detector. The muon radiates at the Cherenkov angle of 41° in water, which allows reconstruction of the track from timing of photon hits if the scattering of light in the detector is not too severe. Above the critical energy, stochastic losses by bremsstrahlung and hadronic interactions of muons become increasingly important. Because only the energy deposited by the muon as it passes through the detector can be measured, the energy of the neutrino can only be determined on a statistical basis, and the relation depends on the spectrum of the neutrino, as discussed above in connection with Figure 18.2.

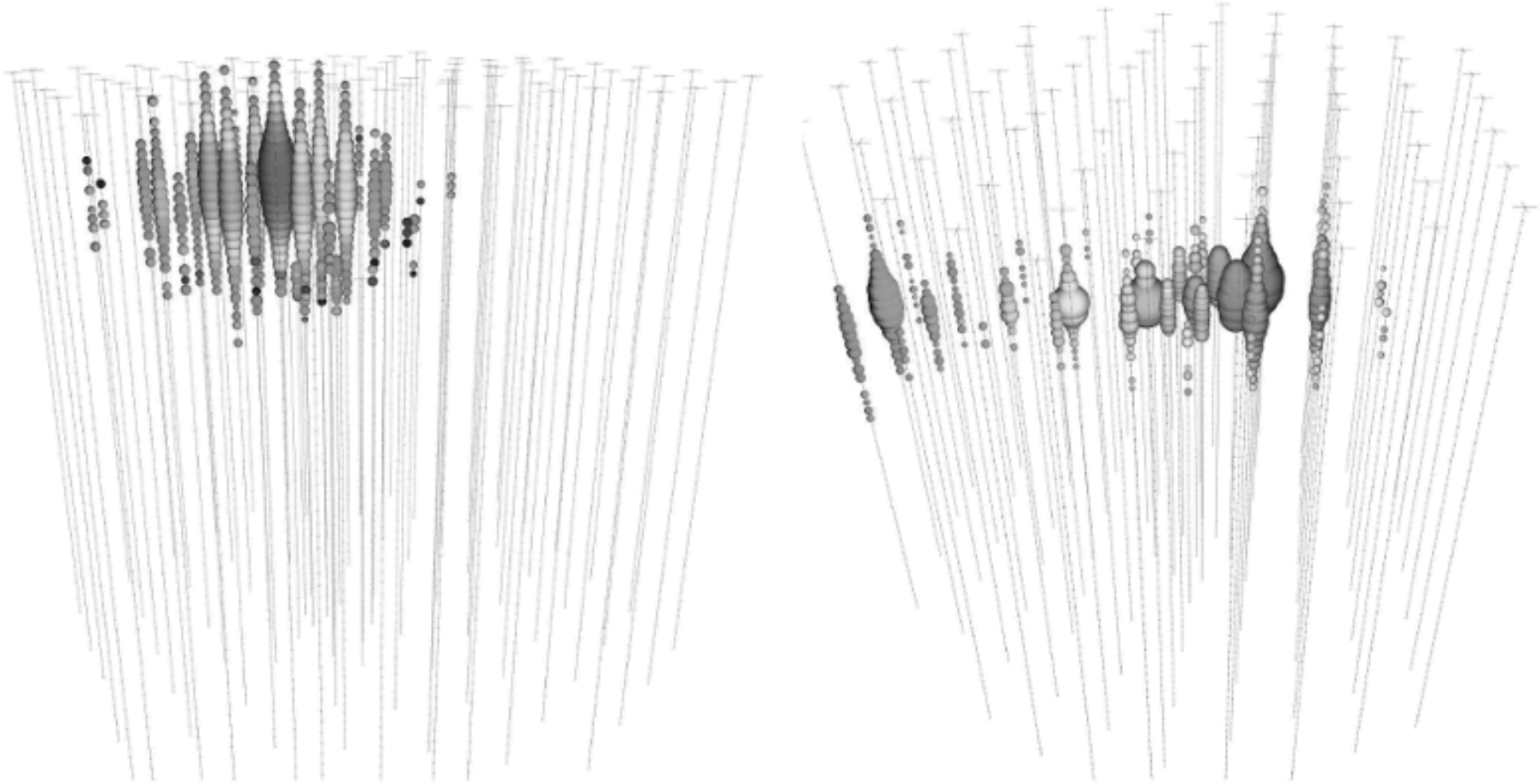

Figure 18.3 Left: Cascade event #35 [327] (2 PeV deposited energy); Right: Starting track event #5 [713] (70 TeV deposited energy). The cascade starts inside the top half of the detector and expands from its center. The track starts inside the detector on the right and moves across. Event displays courtesy of the IceCube Collaboration.

Cascades are produced by charged-current interactions of electron and tau neutrinos and by neutral current interactions of all flavors inside or near the detector. The charged current interaction of an electron neutrino produces a forward electromagnetic cascade, which carries most of the energy of the neutrino, and a hadronic cascade from the nuclear fragments with the remaining $\sim$ 20% of the neutrino energy. In this case, the full energy of the neutrino is deposited in the detector. Neutral current interactions produce only the hadronic cascade, with most of the energy typically carried away by the scattered neutrino. Cascades have a characteristic length of 1000 g/cm^2 for both the electromagnetic component (see Figure 15.2) and the hadronic component (Figure 16.9). This corresponds to 10 m in water or ice, which is less than the typical spacing of optical modules in a large neutrino detector. Angular resolution is therefore not as good for cascades as for tracks. On the other hand, since most of the energy is contained in the detector, energy resolution is better.

The charged current interaction of a ν_τ is a special case because of the properties of the τ-lepton that is produced. A hadronic cascade is generated at the neutrino vertex with much of the neutrino energy going into the τ-lepton, which has a short path length ($\gamma c\tau_\tau \approx 50$ m for $E_\tau = 1$ PeV). For lower energies, the CC interaction of a ν_τ is almost like a single hadronic cascade because the τ has a large branching ratio to hadrons. It also has a branching ratio of 17% to $\mu\nu\nu$ and 20% to $e\nu\nu(\gamma)$. In the region $E_\tau \sim$ PeV, the famous double bang signature, in which the production vertex and the decay vertex can be separated [257], should begin to become visible, depending on detector resolution. Because atmospheric τ neutrinos are rare [717],[3] a high-energy τ neutrino would almost certainly be of extraterrestrial origin.

18.5 Searching for point sources of neutrinos

A main goal of neutrino astronomy is to identify sources of particle acceleration in the Universe by taking advantage of the fact that neutrinos propagate unhindered over great distances from their origin. Tracks of neutrino-induced muons can be reconstructed with relatively good accuracy ($< 1^\circ$), and, at high energy, there is little deviation between the direction of the neutrino and that of the muon. In addition, for detectors of kilometer scale or less, the rate of neutrino-induced muons is greater than the detection rate for other flavors. It is therefore not surprising that this channel is the default in the search for point sources of neutrinos.

All the neutrino detectors have produced sky maps of neutrinos to look for statistically significant clusters of events from a given direction. Basically, an $n\,\sigma$ detection requires

$$N_{\text{events}} - N_{\text{atm}} > n \times \sqrt{N_{\text{atm}}} \tag{18.1}$$

from within $\delta\theta$ of a particular direction in the sky, where N_{atm} is the number of atmospheric events in the same bin. The sensitivity for point sources is enhanced by using unbinned likelihood methods that account for the estimated angular uncertainty of each event as well as its energy, which is likely to be higher for an astrophysical neutrino [719]. In addition to the statistical significance in a particular bin, the significance of an excess in a search of the whole sky needs to be corrected for the number of bins searched. In an unbinned, maximum likelihood search of the whole sky the equivalent procedure involves generating many scrambled sky maps drawn from the same event sample to assess the statistical significance of a particular excess [718].

Another approach is therefore to define a catalog of likely sources beforehand and then look for an excess in the direction of each source in the catalog. Figure 18.4 shows the current upper limits from a sample of IceCube data taken over four years [718] and from ANTARES [720] also for four years. The source catalog comprises 14 potential Galactic sources (mostly SNR) and 30 extragalactic objects (mostly AGNs of various types.) The IceCube data cover the whole sky, but the limits for the Southern sky are relatively high because of the large background of atmospheric muons, which requires setting the threshold in visible energy very high. Corresponding limits from ANTARES [720] are shown for declinations $-90^\circ < \delta < 40^\circ$. Sensitivities are shown with broken lines. The solid line shows the 5σ discovery potential for IceCube. The sensitivities are calculated assuming an E_ν^{-2} differential spectrum. Typical limits from IceCube for Northern hemisphere sources are at the level of 2×10^{-9} cm^{-2}s^{-1}.

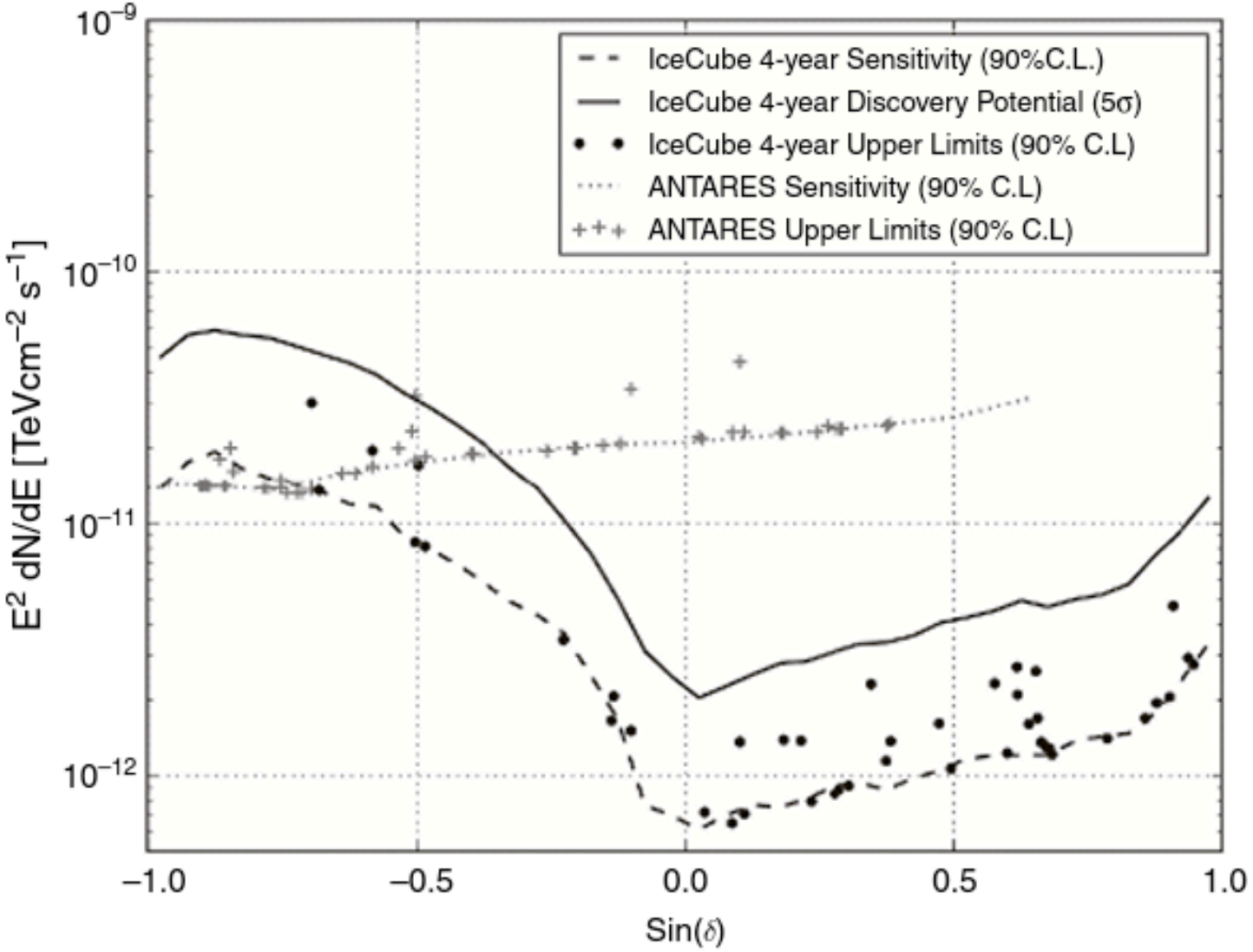

Figure 18.4 Upper limits on neutrinos from selected point sources from IceCube (whole sky) and ANTARES ($\sin(\delta) < 0.64$). From [718], © 2014 by American Astronomical Society, reproduced with permission.

Discussion: The potential of a neutrino telescope to discover an extraterrestrial source of neutrinos above the background of atmospheric neutrinos can be quantified in two ways. The *sensitivity* is defined as the average upper limit that would be obtained in the absence of a signal [721]. The 90% confidence level average upper limit is the "model rejection factor" (mrf). *Model discovery potential* for a particular source/model is sometimes defined as the flux needed to produce a signal with a statistical significance of 5 sigma or more above background in 50% of trials of simulated or randomized background [722].

The use of a reference catalog to search for sources can be further enhanced by looking for coincidences in time with flares observed in various electromagnetic wavelengths in the case of variable sources such as AGNs [723]. The extreme limit of a search for neutrinos associated with flaring sources is the search for neutrinos in coincidence with gamma ray bursts identified by a satellite [724]. At the time of writing this book, no significant point source of high-energy astrophysical neutrinos has been detected.

18.6 Observation of astrophysical neutrinos

The discovery of high-energy astrophysical neutrinos came not from identifying point sources but from an excess of high-energy neutrinos from the whole sky above the steeply falling background of atmospheric neutrinos. It is likely that the observed neutrinos are from unresolved sources in the sky, and the question of when they might be resolved is the subject of the next section.

The classic example of a truly diffuse source of astrophysical neutrinos is provided by the cosmogenic neutrinos from interaction of UHECR in the CMB, as discussed in Chapter 10. The SED of this distribution peaks between 0.5 and 50 EeV. In IceCube the search for such GZK neutrinos starts with a preselected sample of events, each of which has more than 1000 photo-electrons. This sample is further reduced, separately for tracks and cascades, to select events with energies in the range of one PeV and higher. In searching through two years of data (2010–12), two cascade-like events with energies near the threshold of the search were discovered [725]. At $\sim$ 1 PeV their energies are too low to be cosmogenic neutrinos. They were nevertheless at the time the highest-energy neutrinos ever detected.

A dedicated search for events starting inside the detector followed [713], using the same two-year sample of data. Events were required to start in the inner part of the detector by using the outer optical modules as a veto. The fiducial volume is reduced to approximately half the total instrumented volume. Twenty-eight events passed the cuts. The main backgrounds were penetrating muons from above and atmospheric neutrinos from below. It was noted that this method also excludes that fraction of background atmospheric neutrinos with energies sufficiently high to be accompanied in the detector by a muon produced in the same shower.[4] The remaining muon background was estimated from the data by measuring the fraction of events tagged in the outer veto region that are missed by a suitably defined inner veto region. Comparison to calculated backgrounds of atmospheric muons and neutrinos showed an excess at high energy that constitutes the first evidence for high-energy astrophysical neutrinos. A third year of data was examined with the same analysis procedure, confirming the discovery of high-energy astrophysical neutrinos [327]. Assuming a differential spectral index of -2 for the astrophysical component and a flavor ratio on Earth of $1:1:1$, the astrophysical flux per flavor $(\nu + \bar{\nu})$ is

$$E^2\phi(E) = 0.95 \pm 0.3 \times 10^{-8}\ \mathrm{GeV\ s^{-1}sr^{-1}cm^{-2}}. \qquad (18.2)$$

A fit to the astrophysical component without a prior constraint on its spectral index allows spectral indexes from -2.0 to -2.3 depending on the background of prompt neutrinos. The best fit is at the lower boundary of the interval at

$$E^2\phi(E) = 1.5 \times 10^{-8} \left(\frac{E}{100\,\mathrm{TeV}}\right)^{-0.3} \ \mathrm{GeV\ s^{-1}sr^{-1}cm^{-2}}. \qquad (18.3)$$

If the flavor ratio of antineutrinos on Earth is $(\bar{\nu}_e : \bar{\nu}_\mu : \bar{\nu}_\tau) = (1 : 1 : 1)$, the harder spectrum (Eq. 18.2) cannot continue unbroken above the threshold of 6.3 PeV for the Glashow process, $\bar{\nu}_e + e^- \rightarrow W^-$. Three events with energies above 2 PeV would have been expected for an unbroken E^{-2} spectrum [327].

Discussion: In 1960 Sheldon Glashow pointed out that the electron antineutrino should have a resonant interaction with the electron at the mass of the W^- vector boson [98]. From simple kinematics, with $M_W = 80$ GeV the resonance is at a $\bar{\nu}_e$ energy of 6.3 PeV in the lab system. The total cross section in the resonance region is given explicitly in Eq. 3.47 and the differential cross section in Eq. 3.48. When he wrote the paper, the mass of the W was not known and its existence was still a theoretical conjecture, so he was hoping the process would show up at lower energy and reveal the massive vector boson. Glashow pointed out that if the weak vector boson had the same mass as the kaon, the resonance would occur at 2 TeV and could be observed in a relatively small neutrino detector.

In light of the IceCube observation of high-energy astrophysical neutrinos, the use of the Glashow resonance as a diagnostic is again of great interest [726]. For example, if a large fraction of the signal is from

$$p + \gamma \rightarrow \Delta^+ \rightarrow \pi^+ n \rightarrow \mu^+ \nu_\mu,$$

then there could be a significant asymmetry between the ν_e and $\bar{\nu}_e$, similar to the situation for cosmogenic neutrinos in Figure 10.5. The μ^+ decay gives a $\bar{\nu}_\mu$ and a ν_e at high energy, but the $\bar{\nu}_e$ from neutron decay is at much lower energy. Some $\bar{\nu}_e$ would be produced at high energy from non-resonant photoproduction processes, but the starting ratio of $\bar{\nu}_e/\bar{\nu}_\mu$ would be small.

The starting event analysis described above was extended to lower energy by defining a set of nested veto regions, with more stringent cuts as energy decreased [727]. The innermost region corresponds to a threshold in deposited energy of about 1 TeV. The two-year data sample in this analysis includes 283 cascades and 105 starting tracks. With the assumption of a single power law, the fit to the astrophysical component is

$$E^2\phi(E) = 2.06^{+0.35}_{-0.26} \times 10^{-8} \left(\frac{E}{100\,\mathrm{TeV}}\right)^{-0.46\pm0.12} \mathrm{GeV\ s^{-1}sr^{-1}cm^{-2}}. \quad (18.4)$$

A noticeable feature of the IceCube astrophysical neutrino candidates in the high-energy starting event (HESE) analysis is that most of the events are cascades, although the signal does include a fraction of high-energy starting tracks. The excess of cascades is due largely to the energy selection threshold. Charged-current interactions of electron neutrinos and a large fraction of charged-current interactions of τ-neutrinos deposit the full neutrino energy in the detector. In contrast, for starting tracks (CC interactions of ν_μ), much of the energy is carried out of the detector by the muon. In this situation, it is important to note that evidence for a high-energy astrophysical component also appears in the neutrino-induced muon sample from below the horizon in IceCube [728]. Although it is not yet possible to make a precise measurement of the neutrino flavor ratio with IceCube, two analyses [729, 730] show that the observed track/cascade ratio is consistent with a ratio $(\nu_e{:}\nu_\mu{:}\nu_\tau) = (1{:}1{:}1)$ on Earth.

Discussion: Figure 18.5 is a triangular display of the three neutrino flavor space. This diagram has the property that the sum of the three perpendicular distances to the sides is unity for any point inside the triangle. The fraction of each neutrino flavor is proportional to the perpendicular distance from the side of the triangle opposite the vertex for that flavor.

Points for three specific ratios at the source are shown by the symbols along the right side: square for $(\nu_e : \nu_\mu : \nu_\tau) = (0 : 1 : 0)$; circle for $(1 : 2 : 0)$ and triangle for $(1 : 0 : 0)$. After oscillation averaging over astrophysical distances, the expected values for these three initial points move to the center as shown by the dashed arrows. The entire allowed region on Earth for standard, three-flavor neutrino oscillations is confined to a narrow region that connects the three exemplary values of the source ratio. The allowed region has nearly equal fractions of ν_μ and ν_τ, while the fraction of ν_e has a larger range of possible values. Note that neutrinos and antineutrinos do not mix, so the physics at the source should be considered separately for neutrinos and antineutrinos.

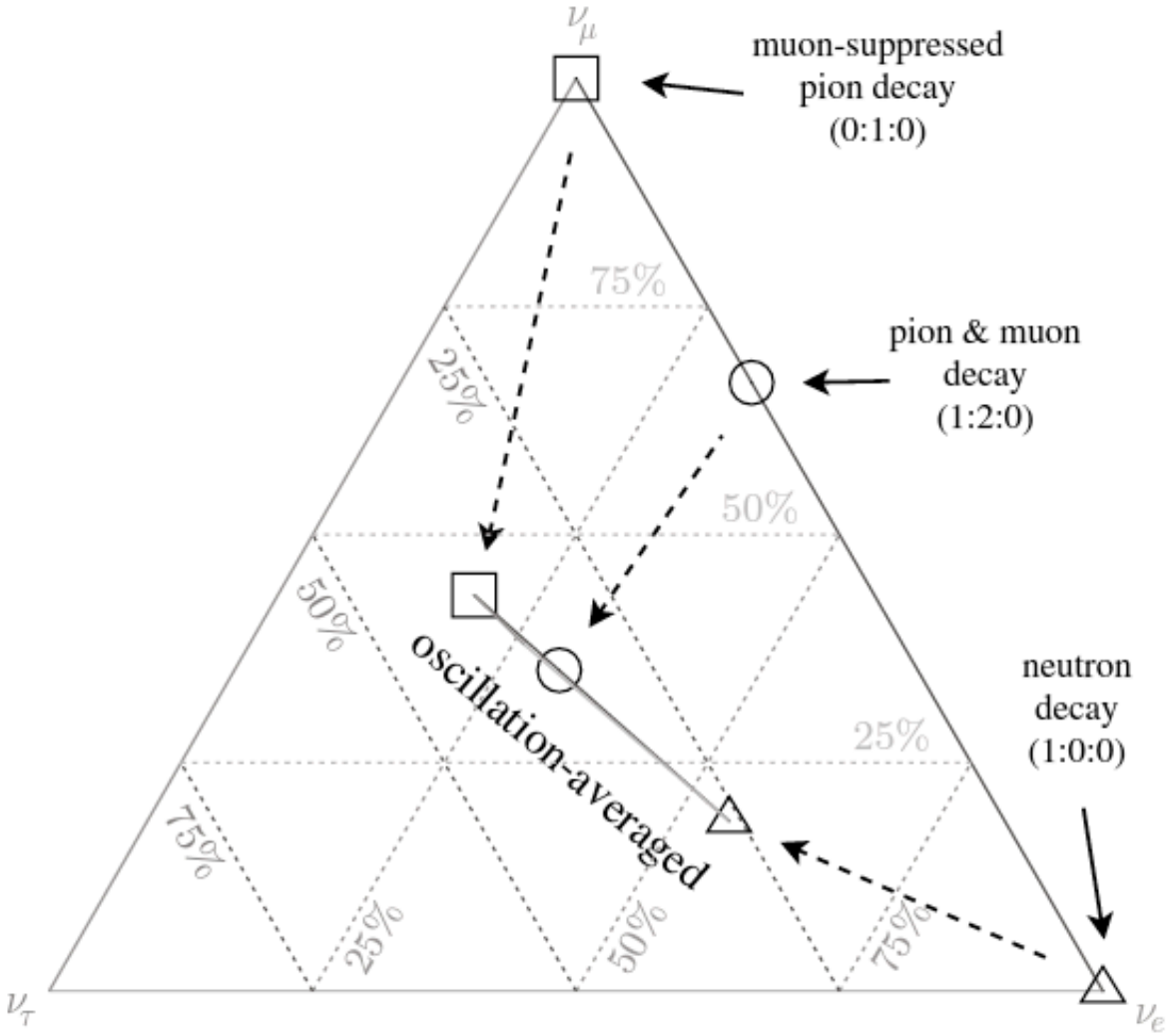

Figure 18.5 Neutrino flavor triangle (courtesy of Markus Ahlers and the IceCube Collaboration [716]). The diagram shows the range of possible flavor ratios on Earth as the width of the line labeled "oscillation-averaged." See text for discussion.

18.7 Sources of astrophysical neutrinos

Potential sources of high-energy cosmic rays are also likely candidates for sources of astrophysical neutrinos. For galactic sources such as supernova remnants, pulsar wind nebulae and accreting binaries, the connection is straightforward. Such sources will eventually be revealed by an excess of neutrinos over the atmospheric background similar to the way in which galactic sources of TeV gamma rays have been identified.

Potential extragalactic sources need a separate discussion. One problem for neutrino astronomy was understood from the beginning, which is the large target volume needed to overcome the low neutrino interaction cross section. The positive side of this problem is that neutrinos escape from deep inside energetic sources and propagate without deviation from the edge of the Universe. The latter point is also problematic in the sense that the observed extragalactic signal may be from a large number of weak sources, many of which are at large red shift [731].[5]

This situation can be quantified by comparing the total power needed to provide a given signal with the typical luminosity per source for a given population of potential sources.

Suppose there is a class of sources with typical luminosity in neutrinos L_ν erg/s with a density in space of ρ. Then the total rate of neutrinos per unit area will be

$$F_\nu = \int L_\nu \rho \frac{\mathrm{d}^3 r}{4\pi r^2} = \frac{1}{4\pi} \int L_\nu \rho \mathrm{d}\Omega \mathrm{d}r. \tag{18.5}$$

The flux per steradian is obtained by integrating over distance, with the result

$$\frac{\mathrm{d}F_\nu}{\mathrm{d}\Omega} = \xi \frac{L_\nu \rho R_H}{4\pi}, \tag{18.6}$$

where the Hubble radius is

$$\frac{c}{H_0} = \frac{3 \times 10^5 \mathrm{km/s}}{72\,\mathrm{km/s/Mpc}} \approx 4000\,\mathrm{Mpc}$$

and ξ is a factor (usually $\sim$ 2 or 3) that accounts for the cosmological evolution of the sources [732]. If we equate this to the flux observed by IceCube, we have

$$\xi \frac{L_\nu \rho R_H}{4\pi} = \frac{E_\nu \mathrm{d}N_\nu}{\mathrm{d}\Omega\, \mathrm{d}\ln(E_\nu)} = 2.8 \times 10^{-8} \frac{\mathrm{GeV}}{\mathrm{cm^2 s\ sr}} = 1.3 \times 10^{46} \frac{\mathrm{erg}}{\mathrm{Mpc^2 yr\ sr}}, \tag{18.7}$$

where the flux is normalized to the IceCube measurement [327] for the sum of all three neutrino flavors assuming an E^{-2} spectrum.

Inverting Eq. 18.7 gives the minimum power-density needed to produce the observed neutrino flux as

$$\rho\, L_\nu = \frac{4 \times 10^{43}}{\xi} \frac{\mathrm{erg}}{\mathrm{Mpc^3 yr}} \sim 10^{43} \frac{\mathrm{erg}}{\mathrm{Mpc^3 yr}}. \tag{18.8}$$

Viable sources must be above a line in luminosity–density space, otherwise they are not sufficiently luminous to produce the observed flux. Such a plot is shown in

Figure 18.6 following the suggestion of Kowalski [733]. The Kowalski plot for cosmic neutrinos is in some ways analogous to the Hillas plot for extragalactic cosmic rays. The source classes shown are subsets of the categories listed in Table 17.1 as possible sources of UHECR. The intrinsic luminosity numbers in the plot here are significantly larger than the minimum required for the UHECR in the case of galaxy clusters and the BL-Lac and FR II classes of AGN. The density of starburst galaxies is $\sim$ 10% of the density of all galaxies. The solid line shows the minimum total neutrino luminosity needed to provide the flux per flavor of Eq. 18.2. The broken line shows the minimum luminosity if the efficiency for neutrino production is 1% of the total.

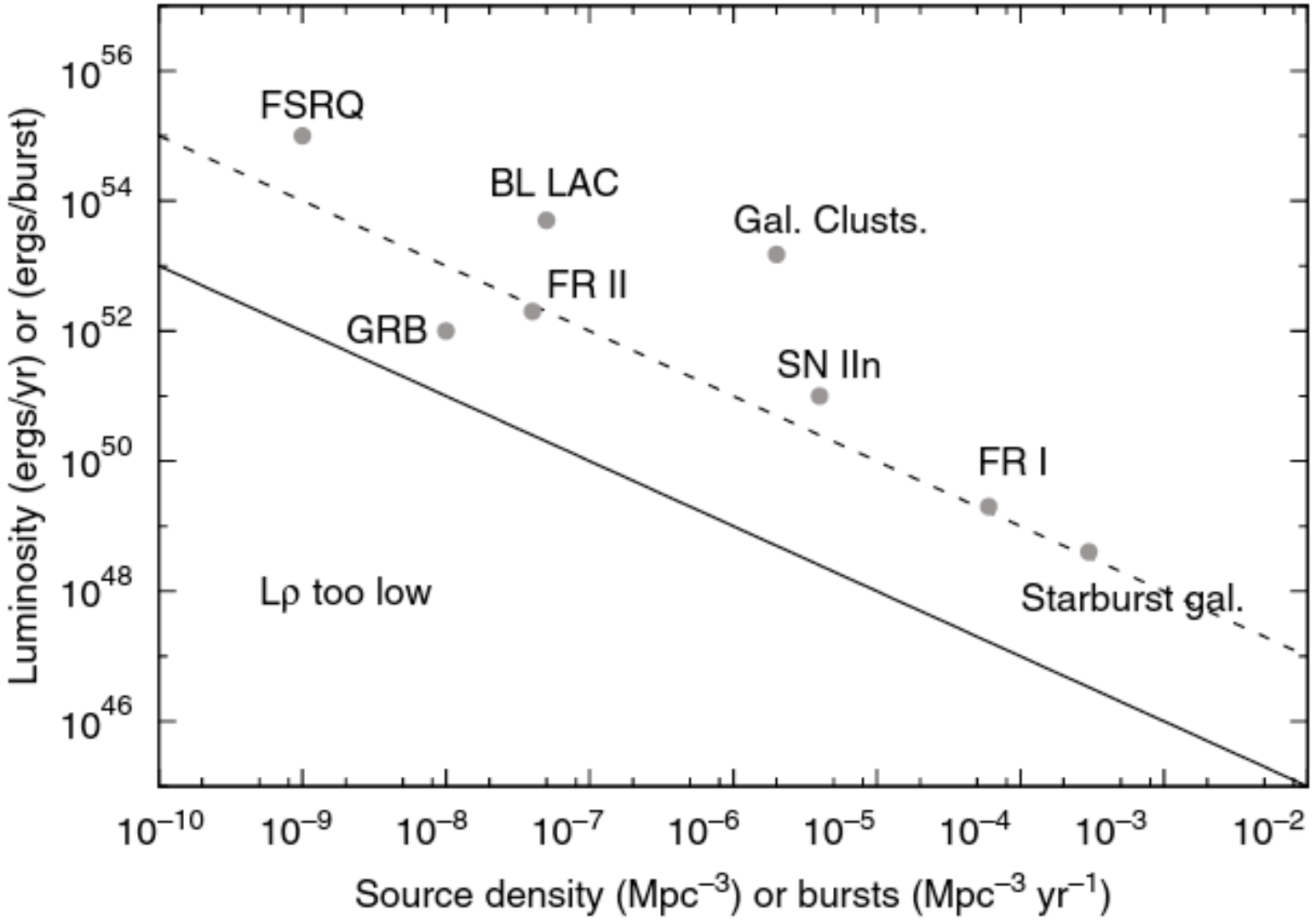

Figure 18.6 Luminosity vs density for potential sources of high-energy astrophysical neutrinos. This figure is modeled after the diagram introduced by Kowalski [733]. See text for explanation and discussion.

Discussion: In the analysis above we have evaluated the differential power requirement per logarithmic interval of energy at an unspecified energy. The astrophysical flux in IceCube emerges from the background above 100 TeV. The total power requirement is obtained by integrating over energy, so it depends on the extent of the astrophysical spectrum and on its shape. For a spectrum with a differential index of -2 the integral is proportional to $\ln(E_{\rm max}/E_{\rm min})$. For a steeper spectrum, however, the total power requirement will be larger, with the value dominated by the lower limit of the integration. If the neutrinos are produced by cosmic ray interactions with gas, $E_{\rm min} \sim 1$ GeV. However, if they are produced in interaction of protons with photons in the source region, $E_{\rm min}$ will depend on the temperature of the target photon distribution and can be much larger. In addition, the normalization in Figure 18.6 assumes the IceCube astrophysical neutrino flux is entirely extragalactic, which may not be the case. At the time of writing, the contribution of Galactic sources to the observed spectrum in IceCube is not known, though it is likely to be a relatively small fraction of the total because many of the high-energy events come from far away from the Galactic plane. The shape of the spectrum is also not yet certain. A hard spectrum with a high-energy cutoff is possible, but a steeper spectrum, possibly with a low-energy cutoff, is also possible. A more detailed analysis would take into account the expected spectral properties of each class of neutrino source and focus on the power requirement in the region of $\sim$ 100 TeV, as indicated by the fits in Eqs. 18.3 and 18.4.

Not all the source classes above the line in Figure 18.6 are equally likely as potential sources of the high-energy astrophysical neutrinos observed by IceCube. For example, as of 2015 no high-energy neutrinos have been observed in coincidence (space and time) with more than 500 potentially visible GRBs [724] even though several coincidences should have been seen in some standard models in which GRB are normalized to produce the observed UHECR. One generic idea for a compact cosmic accelerator is that the protons being accelerated would be confined in the magnetic fields essential for acceleration. When the protons interact in the intense internal radiation fields, secondary protons from $p + \gamma \rightarrow p + \pi^0 X$ would remain in the accelerator, while neutrons from $p + \gamma \rightarrow n + \pi^+ X$ could escape from the system. The neutrons would decay and contribute to the population of UHECR protons, while $\pi^+ \rightarrow \mu^+ \nu_\mu$ and the subsequent muon decay would generate a flux of neutrinos related by kinematics to the cosmic rays from neutron decay. Such a model normalized to produce the observed flux of UHECR [734] is ruled out by the non-observation of GRB with IceCube [724].

Constraints can also be obtained on steady sources by comparing the upper limits from Figure 18.4 with what might be expected from nearby sources. Taking $d \sim (4\pi\rho)^{-1/3}$ as an estimate of the distance to a nearby source of a population of density ρ, we can estimate the flux as

$$F_\nu \approx \frac{L_\nu}{4\pi d^2} = \frac{L_\nu d}{4\pi d^3} = L_\nu \rho d. \tag{18.9}$$

A typical upper limit for a point source in the Northern hemisphere from Figure 18.4 is $F_\nu^{u.l.} \leqslant 2 \times 10^{-9}$ GeV/cm^{2}s. From Eq. 18.9 we then have

$$d \approx (4\pi\rho)^{-1/3} \leqslant \frac{F_\nu^{u.l.}}{L_\nu \rho}. \tag{18.10}$$

Inserting the numerical estimate of the point source upper limits and the observed luminosity density then gives the following estimates for the upper limit on the distance to a nearby point source and the corresponding lower limit on the source density allowed by the non-observation of point sources:

$$d \leqslant 100\,\text{Mpc} \quad \text{and} \quad \rho \geqslant 10^{-7}\,\text{Mpc}^{-3}. \tag{18.11}$$

This lower limit for the source density is slightly above the expectation for the blazar population (BL-Lac and FR II) in Figure 18.6.

18.8 Multi-messenger astronomy

One possible class of sources that satisfies the constraint of Eq. 18.11 is the subset of starburst galaxies, which we discussed briefly in Section 11.7. Two nearby starburst galaxies have been detected as weak ($<$ 1% Crab) TeV γ-ray sources, M82 at 4 Mpc [735] and NGC 253 at 2.5 Mpc [736, 737]. Observations of γ-radiation from starburst galaxies with the Fermi satellite [356] are interpreted in Figures 11.6 and 11.7 as arising from cosmic ray interactions in the dense environment of these galaxies. As the rate of star formation increases, the production of γ-rays approaches the calorimetric limit in which the cosmic rays all interact and lose energy rather than diffusing out of the galaxy. In this limit, the cosmic rays inside the galaxy retain the source spectrum, unlike the case in the Milky Way where the observed spectrum is steeper than the source spectrum because of energy-dependent escape into interstellar space. Therefore the π^0 decay photons produced by cosmic ray interaction in starburst galaxies, as well as the corresponding neutrinos from decay $\pi^{\pm}$ could be expected to have a relatively hard spectrum.

Before the recent observations by IceCube, Loeb and Waxman [679] suggested that, because of their properties, starburst galaxies could be an important source of high-energy astrophysical neutrinos. Moreover, they estimated that the level of the neutrino flux would be comparable to the level of the Waxman–Bahcall limit, even though the limit does not in general apply in this situation where the source is not transparent to the cosmic rays producing the neutrinos. Since the IceCube discovery of an unresolved flux of neutrinos at this level, this possibility has therefore received a great deal of attention.

The basic idea can be understood from the simple propagation equations in Chapter 9. From Eq. 9.15, the differential flux of cosmic rays outside the sources, but inside the galaxy is

$$\frac{\mathrm{d}N}{\mathrm{d}E} = \frac{c}{4\pi} \frac{Q_p(E)\tau_{\mathrm{esc}}(E)}{1 + \lambda_{\mathrm{esc}}(E)/\lambda_p}, \tag{18.12}$$

where the equation is written here assuming protons at high energy for which $R \approx E$. The proton interaction length in hydrogen at high energy is $\approx 45\,\mathrm{g/cm^2}$. In the Milky Way, from Eq. 9.13, $\lambda_{\mathrm{esc}} = \beta\, c\, \rho\, \tau_{\mathrm{esc}} \approx 5\ \mathrm{g/cm^2}$ around 30 GeV and decreases further as energy increases. Thus, in the Milky Way, the energy loss by re-interaction is negligible for protons, and the cosmic ray flux in the

ISM is steeper than the source spectrum, characterized by the decreasing value of τ_{esc} in the numerator of Eq. 18.12. In starburst galaxies, however, densities and magnetic fields are both higher, so the situation is different. For example, the gas density in the disk is estimated as $\approx$ 200 hydrogen atoms/cm^3 [738]. In addition, up to relatively high energy, cosmic ray escape from a starburst galaxy is dominated by advection rather than diffusion [739]. With a galactic wind of $v_w \sim 1500\,\mathrm{km/s}$ and a scale height estimated at $H \sim 300\,\mathrm{pc}$, the characteristic escape time is constant at $\tau_{esc} = H/v_w \approx 6 \times 10^{12}\,\mathrm{s}$. A detailed estimate of diffusion in a starburst galaxy [739] has a diffusive escape time that is greater than the advective loss time for $E < 5\,\mathrm{PeV}$. Below this energy, therefore, we can estimate $\lambda_{esc} = \beta\, c\, \rho\, \tau_{esc} \approx 60\ \mathrm{g/cm^2}$. Up to $\sim 5\,\mathrm{PeV}$ then the spectrum of cosmic rays in a starburst galaxy has the same shape as the source spectrum, and high-energy protons typically interact once before escaping from the galaxy. At higher energy, diffusion takes over and the spectrum begins to steepen and the probability of interaction to decrease.

Senno et al. [739] provide a detailed model of cosmic ray acceleration by hypernovae and supernovae in starburst galaxies and show that it is possible to obtain the level of neutrino flux observed by IceCube (e.g. Eq. 18.3). There is an important caveat to this model. If the spectrum is too steep, the photons produced along with the neutrinos will exceed the diffuse γ-ray flux observed by the Fermi satellite [740]. Murase et al. [738] estimate that the differential spectral index of the pions producing cosmic rays in the starburst galaxies is constrained to $\alpha < 2.2$. Correspondingly, Senno et al. [739] find that the cosmic ray acceleration in the starburst galaxies must be dominated by hypernovae capable of accelerating protons with a hard spectrum to $\sim 10^{17}$ eV. Too large a contribution from ordinary supernovae, with a lower $E_{\max}$, would produce too many γ-rays if their power were normalized to the > 100 TeV neutrinos of IceCube. Turning this argument around, if the IceCube neutrino spectrum is as steep as Eq. 18.4, then it would not be possible to explain the entire flux with the starburst model.

We can anticipate that the understanding of the high-energy astrophysical neutrino flux observed by IceCube will gradually be clarified. With more data it will eventually be possible to discern separate populations in the spectrum if they exist. More data may also lead to identification of specific sources.